



OPEN ACCESS

EDITED BY

Hugo A. Machado Fernandes,
University of Coimbra, Portugal

REVIEWED BY

Changlu Xu,
University of California, Los Angeles,
United States
Iram Maqsood,
University of Maryland, United States

*CORRESPONDENCE

Victoria Moreno-Manzano,
✉ vmorenom@cipf.es

RECEIVED 22 September 2023

ACCEPTED 27 October 2023

PUBLISHED 13 November 2023


CITATION

Sánchez-Martin MdM, Giraldo E,
Gisbert Roca F, Alastrue-Agudo A,
Martínez-Ramos C, Monleón Pradas M
and Moreno-Manzano V (2023), Acute
transplantation of NPC on electrospun
poly-lactic acid membranes containing
curcumin into the injured spinal cord
reduces neuronal degeneration.
Front. Front. Biomater. Sci. 2:1298894.
doi: 10.3389/fbiom.2023.1298894

COPYRIGHT

© 2023 Sánchez-Martin, Giraldo, Gisbert
Roca, Alastrue-Agudo, Martínez-Ramos,
Monleón Pradas and Moreno-Manzano.
This is an open-access article distributed
under the terms of the [Creative
Commons Attribution License \(CC BY\)](#).
The use, distribution or reproduction in
other forums is permitted, provided the
original author(s) and the copyright
owner(s) are credited and that the original
publication in this journal is cited, in
accordance with accepted academic
practice. No use, distribution or
reproduction is permitted which does not
comply with these terms.

Acute transplantation of NPC on electrospun poly-lactic acid membranes containing curcumin into the injured spinal cord reduces neuronal degeneration

María del Mar Sánchez-Martín¹, Esther Giraldo^{1,2,3},
Fernando Gisbert Roca⁴, Ana Alastrue-Agudo¹,
Cristina Martínez-Ramos^{4,5}, Manuel Monleón Pradas⁴ and
Victoria Moreno-Manzano  ^{1*}

¹Neuronal and Tissue Regeneration Laboratory, Centro de Investigación Príncipe Felipe, Valencia, Spain, ²Department of Biotechnology, Universitat Politècnica de València, Valencia, Spain, ³UPV-CIPF Joint Research Unit Disease Mechanisms and Nanomedicine, Centro de Investigación Príncipe Felipe, Valencia, Spain, ⁴Center for Biomaterials and Tissue Engineering, Universitat Politècnica de València, Valencia, Spain, ⁵Universitat Jaume I, Unitat Predepartamental de Medicina, Castellón de la Plana, Spain

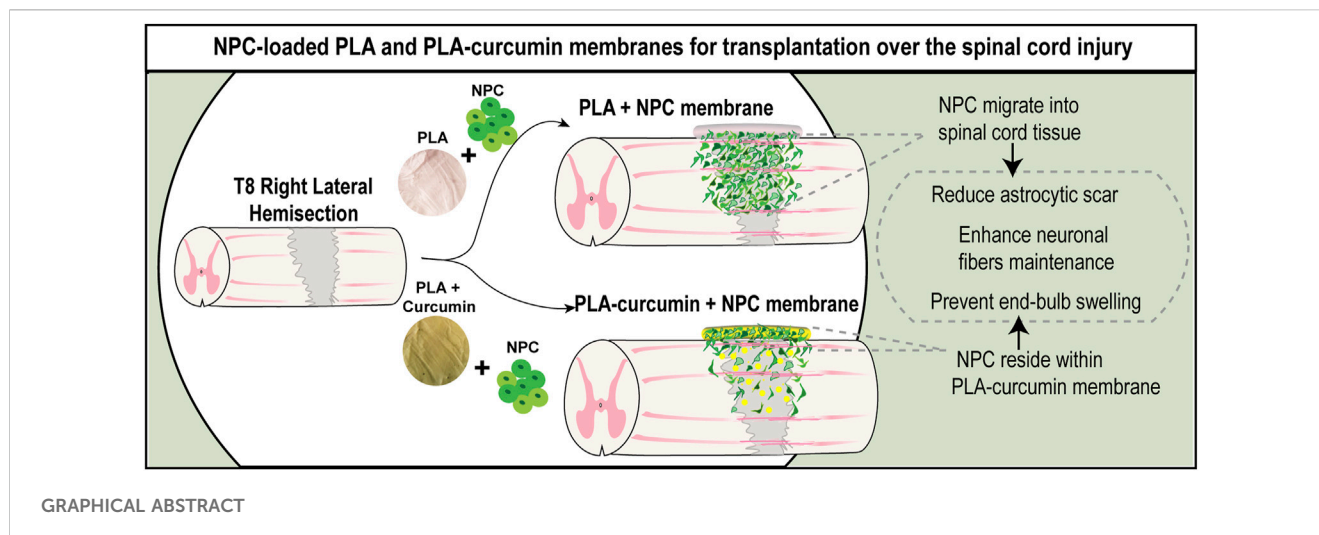
Effective spinal cord injury (SCI) treatment remains a significant challenge, given the complex nature of the primary injury and associated devastating loss of neural activity. Neural progenitor cell (NPC)-based therapy has emerged as a potent strategy for the treatment of SCI. However, the invasive nature of direct cell transplantation and the need to enhance graft integration into host tissue remain critical issues. We implemented an improved combinatorial approach to SCI treatment by functionalizing electrospun poly-lactic acid (PLA) membranes that support the sustained delivery of curcumin (PLA-curcumin) and act as a carrier for NPC for local transplantation. *In vitro* experiments demonstrate that curcumin prevents harmful oxidative and inflammatory stress by preventing death and inhibiting NF- κ B activation (mimicked by treatment with hydrogen peroxide or lipopolysaccharide acid). Curcumin also enhances neurite-like outgrowth in NPC and cortical neurons in culture, which may enhance neural connectivity. *In vivo* transplantation of NPC on a PLA-curcumin electrospun membrane enables cell migration, reduces injured area size, and increases neuronal fiber preservation to induce a slowing of acute neural damage.

KEYWORDS

poly-lactic acid, electrospun membranes, curcumin, NPC, spinal cord injury

Introduction

Spinal cord injury (SCI) is a devastating neurological condition that results in severe motor, sensory, and autonomic dysfunction. Finding effective treatments remains a significant challenge due to the complex pathological cascade that occurs immediately after the primary lesion, typically leading to permanent loss of neuronal activity (Anjum et al., 2020). Addressing singular aspects of the problem will not facilitate successful and functional regeneration after SCI; instead, we require combinatorial treatment strategies that



address multiple SCI-associated problems, which include tissue replacement, inhibitory molecule removal, neurotrophic factor supply, pro-regenerative neuronal signaling pathway manipulation, and neurorehabilitation (Griffin and Bradke, 2020; Zipser et al., 2022).

Scaffolds employed for central nervous system (CNS) repair must meet required biodegradability, topographical, and structural requirements while supporting cell adhesion, and allowing sustained localized release of bioactive molecules (Tsintou et al., 2015; Raynald et al., 2019; Bierman-Duquette et al., 2022). Several biomaterials have proven to be effective in animal models of SCI as implantable bridges or as carriers for drug or cell delivery. The most commonly used natural biomaterials include collagen scaffolds (Zou et al., 2020), hyaluronic acid (Collins and Birkinshaw, 2013), chitosan (Sun et al., 2019), gelatin (Shin and Kang, 2018), alginate (Joung et al., 2018) and fibrin (Jeong et al., 2021). These natural biomaterials have been employed for delivering small compounds or peptides as injectable materials or as scaffolds-forming biomaterials, as reviewed in Jeong et al. (2021). In the realm of synthetic biomaterials, commonly utilized options include poly- ϵ -caprolactone (PCL) (Schnell et al., 2007), polylactic-co-glycolic acid (PLGA) (Santhosh et al., 2017), poly-ethylene glycol (PEG) (Lampe et al., 2010) and poly-lactic acid (PLA) (Zhao et al., 2018). However, the optimal scaffold fabrication and molecule concentration/release period remain poorly described, especially in the context of SCI (Pinelli et al., 2022). Among others materials, poly-lactic acid (PLA) stands out due to its thermoplastic polyester nature, which offers the possibility of creating substrates through 3D printing or electrospinning. This last method is more extensively used and exhibits high biocompatibility, including compatibility with spinal cord tissue (Feng et al., 2023). Furthermore, the versatility of their applications through simple modifications of their physical-chemical structure makes them suitable for small drug delivery (Lasprilla et al., 2012).

Efficient treatment strategies often combine scaffolds and neural progenitor cells (NPC) transplantation to increase grafted NPC survival and better support/guide axonal growth, thereby providing a pro-regenerative environment after SCI (Katoh et al., 2019; Koffler et al., 2019). PLA substrates are suitable for NPC

transplantation allowing adhesion, planar distribution, proliferation, migration, and differentiation (Li et al., 2021; Li et al., 2022) providing a less invasive transplantation and cell delivery method instead of direct injection into the SCI (Zholudeva and Lane, 2019). We recently demonstrated that these materials improved neurite outgrowth and axonal guidance (Gisbert Roca et al., 2020; Gisbert Roca et al., 2021; Gisbert Roca et al., 2022), making them an ideal candidate for NPC delivery and the repair of neuronal tissue damage. Additionally, our research has shown that delivering NPC in combination with curcumin directly to the injured spinal cord can promote neuroprotection and stimulate axonal growth (Requejo-Aguilar et al., 2017; Bonilla et al., 2021; Elkhenany et al., 2021). Curcumin is renowned for its multifaceted biological effects, including antioxidant, anti-inflammatory, and antiapoptotic properties, as documented by Patel et al. (2019). We found that curcumin administration reduces secondary damage after SCI through its anti-inflammatory and anti-oxidative properties, providing neuroprotection, inhibiting neuronal apoptosis, and contributing to functional recovery (Requejo-Aguilar et al., 2017; Bonilla et al., 2021).

In the present study, we implemented and tested in a relevant experimental model, an improved bioengineered-based approach by directly modifying electrospun PLA nanofibers to incorporate soluble curcumin, thereby forming a membrane that serves as a platform for a combinatorial NPC transplantation approach for SCI.

Materials and methods

Preparation of PLA and PLA-curcumin membranes

10 wt% PLA (ME34-GL-000110, Goodfellow GmbH, Hamburg, Germany) was dissolved in a mixture of N, N-dimethylformamide (DMF, 30% v/v, 103034, Sigma Aldrich, Madrid, Spain), and dichloromethane (DCM, 70% v/v CL0329, Scharlab, Madrid, Spain), as previously described and characterized (Ranjeth Kumar Reddy and

Kim, 2018). Curcumin (C1452, Spectrum Chemical Mfg Corp, New York, United States) was dissolved in dimethyl sulfoxide (DMSO, SU0151, Scharlab, Madrid, Spain) at a concentration of 40 mg/mL (108.6 mM). A curcumin-DMSO solution was added to the PLA/DMF/DCM solution, resulting in a final curcumin concentration of 50 μ M. The final solution was stirred for 1 h at 300 rpm at room temperature in the dark due to curcumin's photosensitivity. The solution was then loaded into a syringe (0.15 mm inner diameter) and connected to a high-voltage power supply. Electrospinning parameters were as follows: 20 kV of voltage, a distance of 20 cm from the needle to the collector, and a flow rate of 3 mL/h. To obtain highly aligned nanofibers, the surface onto which the jet was projected was a drum collector turning at a speed of 32 rps. The membranes obtained were dried in a vacuum system to remove solvent traces for 48 h and cut into discs 8 mm in diameter.

In vitro characterization of PLA and PLA-curcumin membranes

The morphology of the electrospinning nanofibers within the generated membranes was studied by field emission scanning electron microscopy (FESEM). Samples were gold-coated for 100 s to provide electrical conductivity. A Zeiss Ultra 55 microscope (Oxford Instruments, Abingdon, United Kingdom) was used to obtain images with an accelerated voltage of 2 kV. The diameter of PLA and PLA-curcumin membranes (100 fibers per group) was measured using the ImageJ software ($n = 3$).

Fourier transform infrared spectroscopy (FTIR) was used to investigate the chemical structure of membranes with attenuated total reflection mode using a Cary 630 FTIR (Agilent Technologies, Santa Clara, CA, United States). Spectra were generated by averaging twenty-four scans at 4 cm^{-1} resolution between 400 cm^{-1} and 4000 cm^{-1} .

Thermal characterization was conducted through thermogravimetric analysis (TGA) using a TGA/SDTA 851 with STARex software (Mettler-Toledo, Barcelona, Spain). Samples were heated from 30°C to 800°C with a rate of 10°C/min. As a result, thermograms were obtained representing the sample's mass loss as a function of temperature and its derivative with respect to temperature. The procedure was performed under a nitrogen flow (N_2) of 20 mL/min and was repeated for three different samples ($n = 3$). The mass fraction of curcumin (ω_{Curc}) was calculated using Eq. 1, where Δm_{Curc} and Δm_{PLA} are the experimental curves of pure curcumin and PLA, respectively.

$$\Delta m_{\text{comp}} = \omega_{\text{Curc}} \cdot \Delta m_{\text{Curc}} + (1 - \omega_{\text{Curc}}) \cdot \Delta m_{\text{PLA}} \quad (1)$$

For the *in vitro* release of curcumin, PLA-curcumin membranes with a diameter of 8 mm were employed and evaluated at various time points over 14 days (1, 3, and 5 h, and 1, 3, 7, 10, and 14 days). The samples were immersed in phosphate-buffered saline containing 0.5% Tween-20 (PBST, pH = 7.4) and agitated at 300 rpm at 37°C. Absorbance at 426 nm was measured in a UV-Vis spectrophotometer (Victor III, Perkin Elmer, Madrid, Spain) to estimate the release of curcumin. [Supplementary Table S1](#) collects a summary of all characterization parameters.

NPC isolation and culture

NPC were harvested from fetal spinal cords of E-15 Sprague-Dawley rats dissected in cold Hank's balanced saline solution (HBSS, 4020091, Gibco, United States) supplemented with penicillin-streptomycin. Dissected tissue was mechanically dissociated by gentle pipetting, and NPC were isolated and cultured as neurospheres in ultra-low attachment plates with growth medium (growth conditions). Specifically, NeuroCult™ Proliferation Medium supplemented with NeuroCult™ Proliferation Supplement (05702, Stemcell Technologies), 100 U/mL penicillin/streptomycin (15070063, ThermoFisher) (DE17-602E, Sigma, ST. Quentin Fallavier Cedex, France), 0.7 U/mL heparin (H3393, Sigma), 20 ng/mL epidermal growth factor (EGF; 10605-HNAE, Thermo Fisher, Horsham, United Kingdom) and 20 ng/mL basic fibroblast growth factor (bFGF; 10014-HNAE, Invitrogen, Massachusetts, United States).

For adherent conditions, NPC were cultured on Matrigel® coated coverslips diluted 1/20 in Modified Eagle's Medium (DMEM)/F12 (11520396, Gibco, Thermo Fisher) in growth medium. To assess spontaneous differentiation of NPC, neurospheres were dissociated with accutase (11599686, StemPro, Thermo Fisher) following the manufacturer's instructions and seeded in a differentiation medium that contains DMEM/F12 supplemented with 100 U/mL penicillin/streptomycin, 2 mM L-glutamine (25030024, Thermofisher), 5 mM HEPES buffer (15630122, Gibco), 0.125% NaHCO_3 , 0.6% glucose, insulin, progesterone, selenite (ITS; 41400045, Gibco) 80 μ g/mL apotransferrin (T1147, Sigma), 60 μ M putrescine (P5780, Sigma), and 2% fetal bovine serum (FBS) and cells were cultured for 1 week.

Isolation and culture of rat cortical neurons

Rat cortical neurons were isolated from the cerebral cortex of E-15 Sprague-Dawley rats, using the same fetal samples as NPC isolation. Dissected tissue was firstly mechanically disaggregated to facilitate the following enzymatic disaggregation with trypsin-EDTA (0.05%, 25300054, Gibco) at 37°C for 10 min. DMEM High glucose (Cytiva HyClone™, Thermo Fisher) supplemented with 10% FBS, and 100 μ g/mL streptomycin were used to dilute trypsin. Then, the tissue was filtered with a sterile cell strainer (70 μ m, Corning Falcon™) and plated directly on the p24 well plates. After 2 h, culture media were changed to Neurobasal medium (21103049, ThermoFisher) supplemented with B27 (2%), Glutamax (35050061, 1%, ThermoFisher), and 100 μ g/mL streptomycin.

Cell viability and cell cytotoxicity assays in NPC and cortical neurons

To evaluate curcumin cytotoxicity in NPC, we used the MTS 3-(4,5-dimethyl-thiazol-2-yl)-5-(3-carboxymethoxyphenyl)-2-(4-sulfo-phenyl)-2H-tetrazolium cell viability assay following the manufacturer's instructions (ab197010, Abcam, Cambridge, United Kingdom). NPC seeded at a density of 1.5×10^4 cells/well in Matrigel-coated 96-well plates were

allowed to attach and expand for 48 h. To perform dose-response experiments, cells were treated with one of the following concentrations of curcumin for 48 h: 1, 5, and 10 μM (C138, Sigma). The optical density was measured in triplicate at 490 nm using a microplate reader Victor 2 (Perkin Elmer Inc., Waltham, Massachusetts, United States) ($n = 3$).

To test the capacity of curcumin to prevent oxidative damage in NPC, a toxic concentration of hydrogen peroxide (7722-84-1, Sigma) was used to mimic the acute oxidative damage occurring at the injury site after SCI. NPC seeded in triplicate at a density of 1.5×10^4 cells/well in Matrigel-coated 96-well plates were allowed to attach and expand for 24 h. NPC were treated for an additional 24 h with 1, 5, or 10 μM of curcumin and then exposed to 75 μM H_2O_2 ; after 4 h incubation, the cell toxicity was measured by MTS assay ($n = 3$).

To evaluate curcumin toxicity in neurons, an exclusion propidium iodide (PI, 25535, Sigma Aldrich) staining assay was employed. Neurons were seeded at a density of 1.5×10^4 cells/well into a poly-L-Lysine (PLL, P2636, Millipore Sigma) coated 96-well plate and allowed to attach and extend for 5 days in the Neurobasal medium. Then, neuronal cultures were treated with different concentrations of curcumin (1, 5, and 10 μM) for 48 h and then incubated with Hoechst 1:1000 (33342, ThermoFisher) and PI 1:1000 in phosphate buffer saline (PBS) for 5 min. Neuronal toxicity was expressed as the percentage of PI-positive neurons normalized to a total number of Hoechst-positive neurons in triplicate ($n = 3$).

NF- κB activation assay in NPC treated with curcumin

To assess the potential anti-inflammatory properties of curcumin, NPC were incubated on Matrigel-coated coverslips in p24 well plates at a density of 4×10^4 cells/well. Cell cultures were then treated with 5 μM curcumin for 24 h and stimulated with 1 $\mu\text{g}/\text{mL}$ of lipopolysaccharide (LPS) (L8274, Sigma-Aldrich) for an additional 24 h to activate NF- κB nuclear translocation. Cells were then evaluated for NF- κB immunostaining; nuclear translocation was quantified from at least ten fields (40x) ($n = 3$).

Neurite outgrowth analysis of NPC and neurons

NPC were seeded at a density of 3×10^4 cells into Matrigel-coated coverslips in a p24 well-plate. Cells were allowed to attach and expand for 24 h in growth medium. Then, NPC cultures were treated with different concentrations of curcumin (1, 5, and 10 μM). Cultures were incubated for 48 h, and neurite outgrowth was quantified using the most extended neurites per cell of at least 50 Nestin-positive cells. NeuriteJ plug-in from ImageJ 1.8.0_172 version was used, as previously described (Torres-Espin et al., 2014).

To assess the potential effect on neurite elongation in neurons, cells were seeded at a density of 3×10^4 cells into Poly-L-lysine-coated glass coverslips in a p24 well-plate. Cells were allowed to attach and expand for 72 h. Then, neuron cultures were treated with

different concentrations of curcumin (1, 5, and 10 μM). Cell cultures were incubated for an additional 48 h, and neurite outgrowth was quantified by measuring the most extended axon projection with the NeuriteJ plug-in of ImageJ 1.8.0_172 version as previously described (Torres-Espin et al., 2014).

NPC culture on PLA and PLA-curcumin membranes

NPC were seeded at a density of 1.2×10^5 on PLA and PLA-curcumin membranes sterilized by γ -radiation (Aragogamma, Spain) using a ^{60}Co radiation source at a dose level of 25 kGy at room temperature in the dark (according to ISO11137). All membranes were previously incubated with Matrigel for 30 min, washed with PBS, and left to dry for up to 5 min. 6×10^4 NPC were embedded into 3 μL of Matrigel at a dilution of 1/5 with growth medium and deposited on top of the membrane surrounded by medium but avoiding floating or immersion to encourage cell attachment during 30 min incubation at 37°C; then, fresh medium was added for cell proliferation or differentiation. Under *in vitro* culture conditions, the volume of the culture medium was adjusted so that PLA-curcumin was released at a concentration of 5 μM .

Immunocytochemical staining, image acquisition, and quantification

Cells were fixed with 4% paraformaldehyde (PFA; P6148, Sigma) in PBS for 10 min, then permeabilized and blocked with 5% normal goat serum (NGS; 31872, Thermo Fisher) and 0.2% Triton X-100 (9036-19-5, Sigma). Cells were incubated overnight at 4°C with primary antibodies against ki67 (α -Rb, 1:400, ab15580, Abcam, Cambridge, United Kingdom), Nestin (α -ms, 1:400, ab6142, Abcam), anti- β -III tubulin (α -ms, 1:400, MO15013, Neuromics, Edina, MN, United States), Olig-2 (1:500 ab33427, Millipore), anti-GFAP (α -RB, 1:1000; PA1-10004, Dako Denmark A/S, Glostrup, Denmark), NF- κB (1:400 SC-8008, Santa Cruz, CA, United States). Secondary antibodies used were either AlexaFluor-488, -555, or -647 (1:400, Invitrogen, Massachusetts, United States) conjugated antibodies against the respective IgG of the primary antibody. DAPI (1:1000, Sigma, Missouri, United States) was used to stain cell nuclei.

Fluorescent images were acquired using a fluorescent microscope (Apotome; Zeiss, Oberkochen, Germany) or a confocal microscope (Leica, Wetzlar, Germany). Consistent exposures were applied for all images, and ImageJ software was used for image analysis.

Spinal cord lateral hemisection, PLA or PLA-curcumin with NPC membrane implantation and sample collection

Female Sprague Dawley rats (~200 g) were bred at the Animal Experimentation Unit of the Research Institute Príncipe Felipe (CIPF, Valencia, Spain). The maintenance and use of all animals were by

guidelines established by the European Communities Council Directive (86/609/ECC) and the Spanish Royal Decree 53/2013. All experimental procedures were approved by the Animal Care and Use Committee of the Research Institute Prince Felipe (2021/VSC/PEA/0032). The experimental protocol included humane endpoint criteria when severe signs of distress were observed. The rats were housed under standard temperature conditions with controlled 12 h light/dark cycles with *ad libitum* access to food and water. All animals were managed by professionally trained staff.

For the surgical interventions, female rats (200 g) were subcutaneously pre-medicated with morphine (2.5 mg/kg) and anesthetized with 2% isoflurane in a continuous oxygen flow of 1 L/min. Laminectomy was performed at the level of T7-T9 to expose the spinal cord at T8 and induce right lateral hemisection using a microdissector, as previously described (Brown and Martinez, 2019). After SCI, animals were distributed into the following groups ($n = 3$): Control (without any transplant), PLA (PLA membrane), PLA-curcumin (PLA-curcumin membrane), PLA + NPC (PLA membrane containing NPC), PLA-curcumin + NPC (PLA-curcumin membrane containing NPC). All animals were subjected to post-surgery care consisting of subcutaneous administration of 5 mg/kg of enrofloxacin for 7 days, 0.1 mg/kg of buprenorphine twice a day for 4 days after each intervention, and 1 mg/kg of tacrolimus (FK506; LC Laboratories, Boston, United States) starting from 1 day before NPC transplantation until the experimental endpoint.

To adjust the size of the membrane to the laminectomy area, the biomaterial was cut to 2×4 mm. NPC at passages three to four were dissociated with accutase for 10 min at 37°C , and 1×10^6 cells were mixed with 2 μL Matrigel diluted at 1/5 with growing medium deposited on top of the membranes and incubated for 30 min to encourage cell attachment before implantation by direct contact with the injured spinal cord injury immediately after injury. Control groups included the matrix mix without NPC.

Two weeks after SCI and implantation, animals were irreversibly anesthetized by intraperitoneal injection of sodium pentobarbital (100 mg/kg) and fentanyl (0.05 mg/kg) and transcardially perfused with 0.9% saline solution and post-fixed in 4% PFA for 2 h and then maintained in 0.1 M phosphate buffer (PB). For further processing, spinal cord tissue was carefully removed, and the thoracic segments, including T6 to T10, were cryopreserved with 30% sucrose.

Histological assessment

After carefully removing meninges, tissues were placed into OCT blocks (Tissue-Tek[®], Sakura Finetek, United States). Spinal segments were cryosectioned into horizontal sections of 20 μm thickness using an HM340E Electronic rotary microtome (VWR International, Barcelona, Spain).

For tissue orientation and general injury/cyst cavity evaluation, every fifth collected section was stained with H&E in ST5010 Autostainer XL (Leica, Wetzlar, Germany) and scanned using an Aperio Versa scanner (Leica, Wetzlar, Germany). H&E staining was used to determine the anatomical structure and general injury/cyst cavity evaluation and quantify the preserved gray matter and white matter 2 weeks after SCI. The preserved gray or white matter was analyzed by quantifying the darker (grey matter) or lighter (white matter) area and the percentage of the total slice area.

Before immunofluorescence, tissue slices were post-fixed for 5 min and then blocked and permeabilized with 0.1% Triton X-100 (9036-19-5, Sigma), 5% horse serum, and 10% FBS in PBS. Immunofluorescence staining was performed by overnight incubation at 4°C with primary antibodies and 1 h with secondary antibodies at room temperature. Primary antibodies used were anti-GFP (α -CK, 1:800, ab13970, Abcam), anti- β -III tubulin, anti-GFAP, -Nestin, and -Olig-2.

Fluorescence images of each spinal cord slice were acquired using an Aperio Versa scanner (Leica Biosystems, Wetzlar, Germany) or a fluorescent microscope (Apotome; Zeiss, Oberkochen, Germany). Images were visualized and quantified with the Image Scope software or ImageJ/Fiji software 1.8.0_172 version.

The injury area was analyzed by quantifying the negative GFAP area and expressed as the percentage of the total slice area depending on the slice deep. For the quantification of GFAP morphology, we use shape descriptors of the GFAP- area using ImageJ software version 1.8.0_172.

To quantify β -III tubulin positive area at the injury site, the specific positive signal was quantified by creating a mask with the threshold tool and using the “analyze particles” function of ImageJ without size restrictions. This result was normalized to the injury site, corresponding to the region of interest of the GFAP negative measured area. To analyze the button-like β -III tubulin positive area, a new mask was created, and a shape descriptors thresh-point applied after using the “analyze particles” function of ImageJ. A roundness factor greater than 0.7 was selected to ensure that all possible fibers were included in the quantification. Data displayed as the percentage of β -III tubulin positive area with a roundness factor higher than 0.7 normalized to the negative GFAP area. AxonTracer ImageJ plug-in was used to assess axon length quantification at the injury site normalized to the corresponding negative GFAP area.

Statistical analyses

Data were represented as mean \pm standard error mean (SEM) and analyzed using Graph Pad Prism Software. Statistics analysis was performed using the Student's t-test or one-way ANOVA, as indicated, using Turkey's multiple comparisons *post hoc* analysis test. p values <0.05 were considered statistically significant.

Results

Electrospun PLA-curcumin membranes for sustained curcumin delivery

Aligned electrospun membranes of PLA were generated, incorporating curcumin dissolved in DMSO at a concentration of 40 mg/mL, resulting in a final concentration of 50 μM when added to 10% PLA in a combination of N, N-dimethylformamide (DMF, 30% v/v) and dichloromethane (DCM, 70% v/v). The electrospinning process involved placing the final solution, including curcumin (PLA-curcumin) or DMSO (PLA), in a syringe (0.15 mm inner diameter) connected by a capillary with a high voltage power supply, as previously described (Gisbert Roca

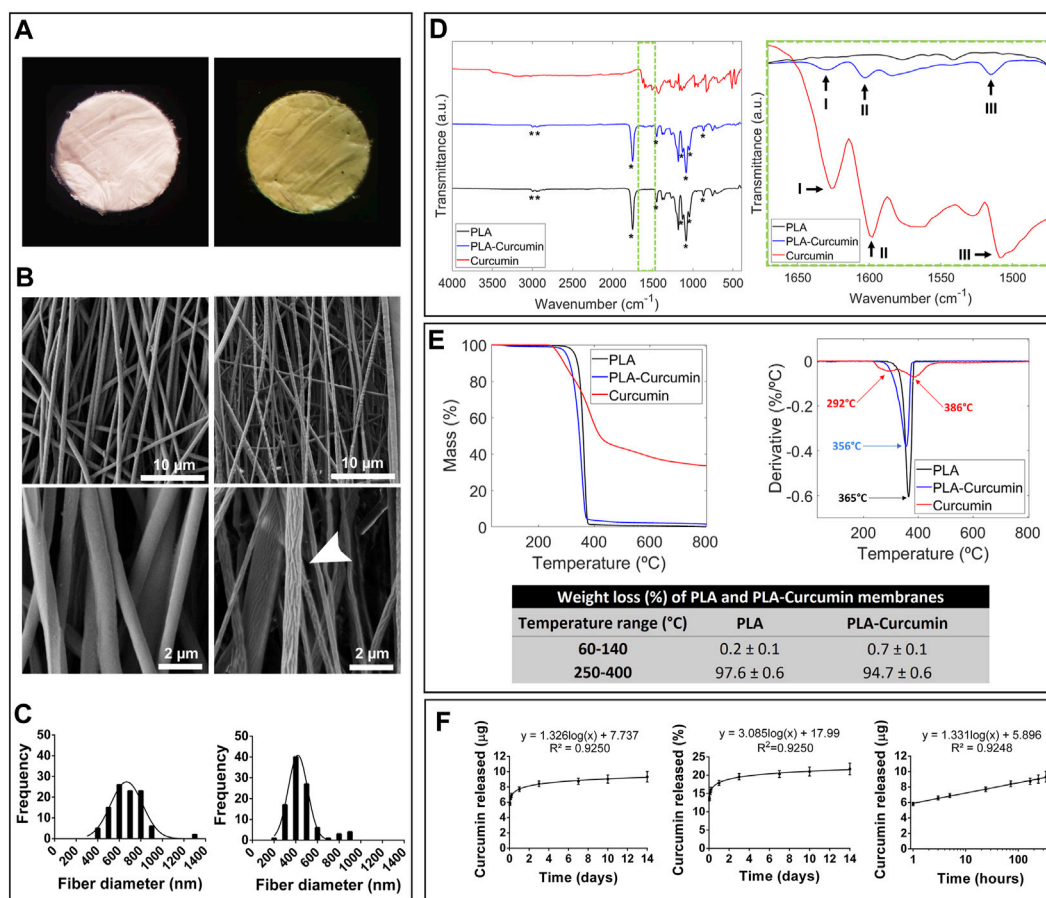


FIGURE 1

Characterization of electrospun PLA and PLA-curcumin membranes. (A) Macroscopic images of PLA (left) and PLA-curcumin (right) circular membranes with a diameter of 8 mm. (B) FESEM images of PLA (left) and PLA-curcumin (right) membranes at low (top) and high magnification (bottom). Scales bar: 10 μm (top), and 2 μm (bottom); (C) Quantification and representation of PLA (left) and PLA-Curcumin (right) membrane fiber diameters as histograms. (D) Chemical characterization of PLA and PLA-curcumin membranes by Fourier transform infrared spectroscopy (FTIR); *Left*: FTIR curves of PLA and PLA-curcumin membranes and unprocessed curcumin, with a star (*) indicating the characteristic peaks of PLA. *Right*: Detail (from the dashed green square from the left panel) of the FTIR curves, indicating the characteristic peaks of curcumin (I, II, III). (E) TGA analysis depicting the heat-dependent loss of mass (*left*) and the derivative (*right*) for PLA and PLA-curcumin membranes. The decomposition temperatures are included in the derivative graph. (F) Curcumin release curves in a PBST solution over fourteen days, left: curcumin mass released (linear representation), center: Percentage of curcumin released with respect to the total amount of curcumin present in the substrate, right: curcumin mass released (logarithmic representation).

et al., 2020). We dried the obtained membranes in a vacuum system to remove solvent traces and then cut membranes into five discs 8 mm in diameter (Figure 1A).

Morphological analysis of the membranes was performed using FESEM, which provided evidence of continuous and aligned fiber composition for both PLA and PLA-curcumin membranes. Under a magnified view in FESEM acquisition, PLA-curcumin membranes displayed higher fiber porosity and roughness than fibers from PLA membranes (Figure 1B, middle panel, white arrow). Quantification of fiber diameter distribution demonstrated the more homogeneously-sized and narrower nature of PLA-curcumin membranes compared to PLA membranes (mean diameters of 470 ± 195 nm and 671 ± 152 nm, respectively) (Figure 1C).

The chemical characterization of PLA and PLA-curcumin membranes was performed using FTIR, confirming the presence of functional groups by identifying characteristic peaks in each sample (Figure 1D). Both membranes displayed PLA peaks

(marked with *), with bands at 2993 cm^{-1} , 2944 cm^{-1} , 1453 cm^{-1} , and 1128 cm^{-1} attributed to the bending and stretching of CH_3 (Ribeiro et al., 2011; Zhang et al., 2016), at 1750 cm^{-1} related to the stretching of $\text{C}=\text{O}$ in the ester group, and at 1084 cm^{-1} , 1043 cm^{-1} , and 868 cm^{-1} attributed to the stretching of $\text{C}-\text{O}$ bonds in the ester group (Ranjeth Kumar Reddy and Kim, 2018). For the PLA-curcumin membrane, we encountered three peaks related to curcumin that overlapped the peaks found for unprocessed curcumin (Figure 1D, right panel): Peak I at 1627 cm^{-1} shows the overlapping stretching vibrations of alkenes ($\text{C}=\text{C}$) and carbonyl ($\text{C}=\text{O}$) groups (Khalil et al., 2014; Chen et al., 2015), Peak II at 1598 cm^{-1} shows the stretching vibration of $\text{C}=\text{C}$ in the aromatic ring of curcumin (Khalil et al., 2014; Chen et al., 2015), while Peak III at 1509 cm^{-1} shows the bending vibrations of benzene ring CH bonds of curcumin (Khalil et al., 2014; Chen et al., 2015). We failed to find any evidence of solvent residues in any sample. In the FTIR analysis we did not identify any new peaks, nor did we see

displacement of the bands of the PLA polar groups. Therefore, we do not identify new significant interactions between both components due to chemical or physical bonds. Since FTIR is a technique sensitive mostly to surface composition the results support the idea that a fraction of curcumin is present in most outer parts of the PLA fibers, without binding to PLA, which is consistent with its release curve.

We evaluated the thermal stability of PLA and PLA-curcumin membranes by TGA (Figure 1E). At low-temperature range (between 60°C and 140°C), both membranes exhibited similar first-stage weight loss ($0.2\% \pm 0.1\%$ and $0.7\% \pm 0.1\%$ of their total weight, respectively) attributed to water loss (Barbosa et al., 2022). During the second stage (between 250°C and 400°C), PLA and PLA-curcumin membranes presented similar thermal degradation ranges, with weight losses of $97.6\% \pm 0.6\%$ and $94.7\% \pm 0.6\%$, respectively, associated with PLA degradation due to breakage of PLA ester bonds (Barbosa et al., 2022). The inclusion of curcumin slightly reduced membrane weight loss by $2.9\% \pm 1.2\%$ in the second stage due to curcumin's slightly higher thermal stability (Figure 1E). The mass fraction of curcumin in the membranes was determined to be approximately 4.3% (Eq. 1).

Finally, we evaluated the gradual release of curcumin from PLA-curcumin membranes immersed in PBS in the presence of 0.5% Tween-20 (PBST, pH = 7.4). The release profile (Figure 1F) showed the amount of curcumin released and the corresponding % of curcumin released with respect to the total curcumin present in the substrate. As observed, there is a primarily burst release of curcumin during the first 48 h, followed by a slower and gradual curcumin release profile over the next 12 days. The mass fraction of curcumin obtained from TGA, together with the release study, allowed us to determine that the amount of curcumin released during the first 24 h represents 17.9% of the total loaded curcumin, while the amount of curcumin released in 14 days represents a 21.7% of the total loaded curcumin. Although the initial mixture of PLA and curcumin is co-dissolved and homogeneous, phase separation occurs during the electrospinning process due to the immiscibility of solidified PLA with curcumin. In a slow evaporation process, most of the curcumin would thus be segregated outside the PLA material. In the electrospinning process, because of the rapid evaporation of the jet and the small size of the nanofibers, a fraction of curcumin is retained within the vitrified amorphous phase of PLA, while another fraction is segregated towards the outer surface, where it accumulates. This twofold state of curcumin explains the initial burst in its release and translates into the peak shown in the derivative of the release curve (Supplementary Figure S1). The rest of the curcumin remains occluded in the PLA matrix and is released following the rate of surface erosion of the PLA fiber, which is much slower and results in a more gradual curcumin release after the initial peak. As previously described (Bogdanova et al., 2023), electrospun PLA degrades at a slow rate, losing about 6% of its weight after 2 weeks in PBS at 37°C, which explains the slow release of curcumin after the initial burst. Since the effect of curcumin is primarily anti-inflammatory, it is beneficial to have an initial rapid release followed by a slower minor release. The release of curcumin is also represented with a logarithmic scale since it is useful for modeling the release kinetics.

Overall, we developed a reproducible methodology to fabricate electrospun PLA membranes modified to release curcumin in a

sustained manner over 2 weeks that possessed increased surface fiber roughness.

Curcumin prevents NPC death in response to oxidative damage and NF- κ B translocation upon lipopolysaccharide treatment

This study aimed to evaluate the tolerance of our spinal cord-derived NPC to increasing concentrations of curcumin in solution (1, 5 and 10 μ M), mimicking the expected concentrations delivered from PLA-Curcumin membranes over time. MTS 3-(4,5-dimethyl-thiazol-2-yl)-5-(3-carboxymethoxy-phenyl)-2-(4-sulfo-phenyl)-2H-tetrazolium cell viability assays revealed that none of the tested concentrations of curcumin (1, 5, and 10 μ M) displayed any cytotoxic effect on NPC after 48 h of incubation under growth conditions when compared to the vehicle-treated (0.5% DMSO) control (Figure 2A), as we previously showed in human NPC (Bonilla et al., 2021).

We then induced acute oxidative damage by exposing NPC pre-treated with 1, 5, or 10 μ M of curcumin for 24 h to high doses of H₂O₂ (75 μ M). The results demonstrated that incubation with 5 or 10 μ M of curcumin significantly prevented the hydrogen peroxide-induced reduction in NPC viability assessed by MTS assay measuring the optical density of triplicates at 490 nm (Figure 2B). We then evaluated Curcumin's ability to inhibit nuclear factor κ B (NF- κ B, p65) translocation to the nucleus induced by LPS to further explore the previously reported anti-inflammatory potential of curcumin in NPC (Narouiepour et al., 2022) since NF- κ B activation plays a crucial role in mediating proinflammation following SCI (Bethea et al., 1998). We pre-treated NPC with vehicle (control) or 5 μ M curcumin, previously shown not to induce cytotoxicity and significantly prevented H₂O toxicity, for 24 h and then added 1 μ g/mL of LPS for an additional 24 h to induce nuclear translocation of NF- κ B (as identified by p65 immunostaining and colocalization with DAPI for nuclear staining) (Figure 2C). While LPS treatment (Vehicle + LPS) significantly increased nuclear NF- κ B translocation compared to the vehicle-treated control (Vehicle), curcumin pre-treatment (curcumin + LPS) significantly inhibited NF- κ B translocation to a level comparable with the vehicle-treated control.

These results suggest that curcumin treatment of NPC can prevent harmful oxidative and inflammatory stress by preventing cell death and inhibiting NF- κ B activation.

Curcumin enhances neurite outgrowth from NPC and cortical neurons

The effect of curcumin on neurite-like projections from cultured NPC, closely related to neuritogenesis (More et al., 2012; Gu et al., 2019), was studied through immunostaining for Nestin, an intermediate filament protein known as a neural stem/progenitor cell marker (Kuramoto et al., 2022). NeuronJ ImageJ plug-in (Meijering et al., 2004) was used for 2D neurite tracing and analysis of elongated neurite-like structures marked by Nestin expression. Quantification of formed cell projections demonstrated a significant promotion of neurite-like outgrowth

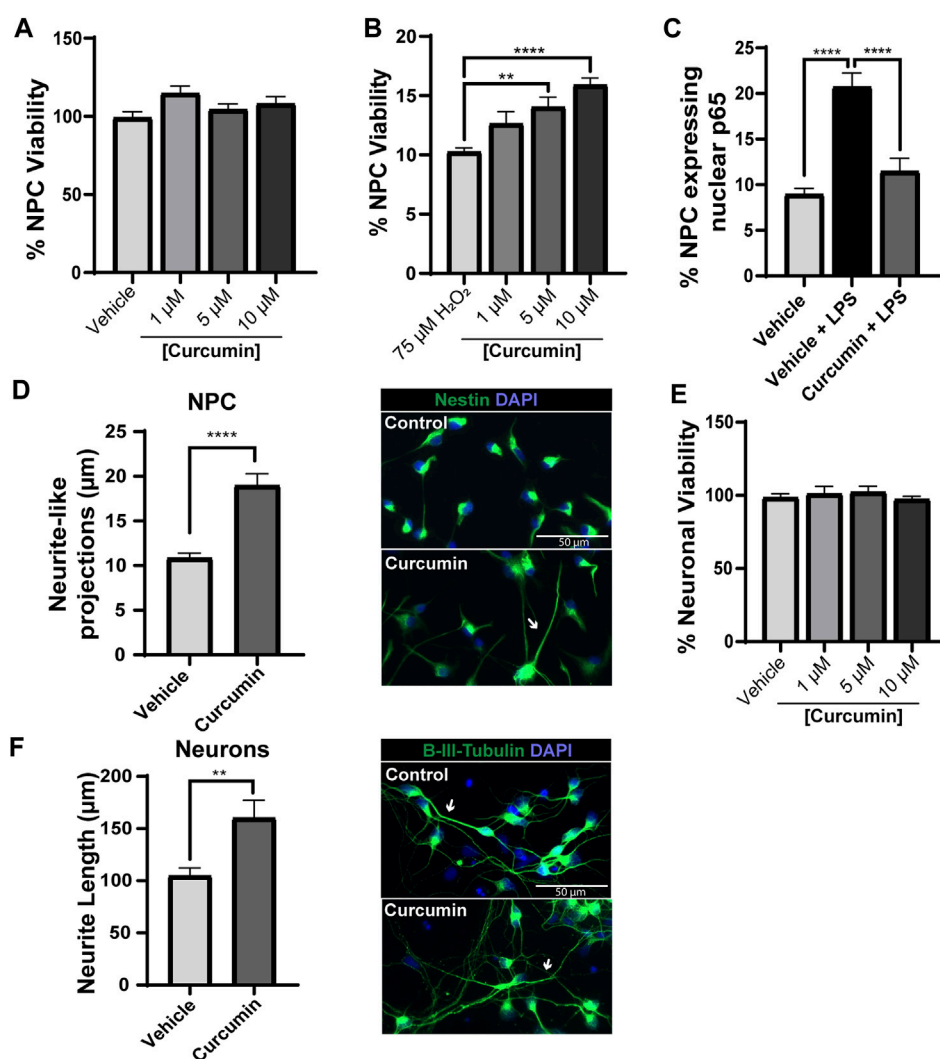


FIGURE 2

Curcumin protects NPC from stress and induces neurite elongation in NPC and mature cortical neurons. **(A)** Viability of curcumin-treated NPC assessed by MTS assay. Data normalized by cell viability in the vehicle-treated control (0.5% DMSO). **(B)** Viability of NPC pre-treated with curcumin for 24 h and then exposed to 75 μM H_2O_2 evaluated by MTS assay. **(C)** Quantification of the number of NPC with nuclear NF- κB p65 expression following 24 h pre-treatment with 0.5% DMSO (Vehicle) or 5 μM curcumin and then 24 h treatment with 1 $\mu\text{g}/\text{mL}$ LPS (Vehicle + LPS; Curcumin + LPS). **(D) Left panel:** Quantification of neurite-like projections from NPC stained with Nestin in the vehicle-treated control (0.5% DMSO) and NPC treated with 5 μM curcumin for 24 h represented as the average neurite length (μm) per cell from at least fifty cells. **Right panels:** Representative images of Nestin immunofluorescence staining (green) and nuclear detection (DAPI, blue) for vehicle-treated control and curcumin treatment. White arrows indicate projections of long neurites. **(E)** Cortical neuron viability after curcumin treatment (1, 5, and 10 μM) for 48 h evaluated by propidium iodide exclusion staining. Data normalized by neuronal viability in the vehicle control group (0.5% DMSO). **(F) Left panel:** Quantification of axon length quantified by β -III tubulin staining in the vehicle-treated control (0.5% DMSO) and cortical neurons treated with 5 μM curcumin for 24 h. **Right panel:** Representative images of β -III tubulin immunofluorescence staining (green) and nuclear detection (DAPI, blue) for vehicle-treated control and curcumin treatment. White arrows indicate long axonal projections. Scale bars = 50 μm , $n = 3$ for each experiment. Data expressed as mean \pm SEM. ** $p < 0.01$, *** $p < 0.001$, and **** $p < 0.0001$ determined by ordinary one-way ANOVA, Sidak's multiple comparisons tests (A–C,E) and Student's t -test (D,F).

in NPC treated with 5 μM curcumin for 24 h compared with vehicle-treated NPC (Figure 2D), suggesting that curcumin induces the development of neurite-like processes with improved neuritogenesis (essential during neuronal regeneration) (Dupraz et al., 2019).

In cultures of mature cortical neurons, none of the tested curcumin concentrations (1, 5, or 10 μM) prompted cytotoxicity after 48 h of treatment compared to the vehicle-treated control, as measured by propidium iodide exclusion assay (Figure 2E). Notably, a 5 μM concentration of curcumin significantly increased neurite outgrowth from cortical neurons, quantified from the most extended

axonal projection in β -III tubulin-stained mature cortical neurons after 3 days of incubation compared with vehicle-treated control neurons (Figure 2F). These data suggest that curcumin also induces neurite outgrowth in mature neurons, which could contribute significantly to neuronal connectivity after SCI.

Overall, local curcumin delivery could improve the survival and engraftment of ectopically transplanted NPC within the hostile microenvironment characteristic of SCI without inducing additional neuronal damage and promoting neuronal elongation, which will contribute to the formation of new neuronal connections.

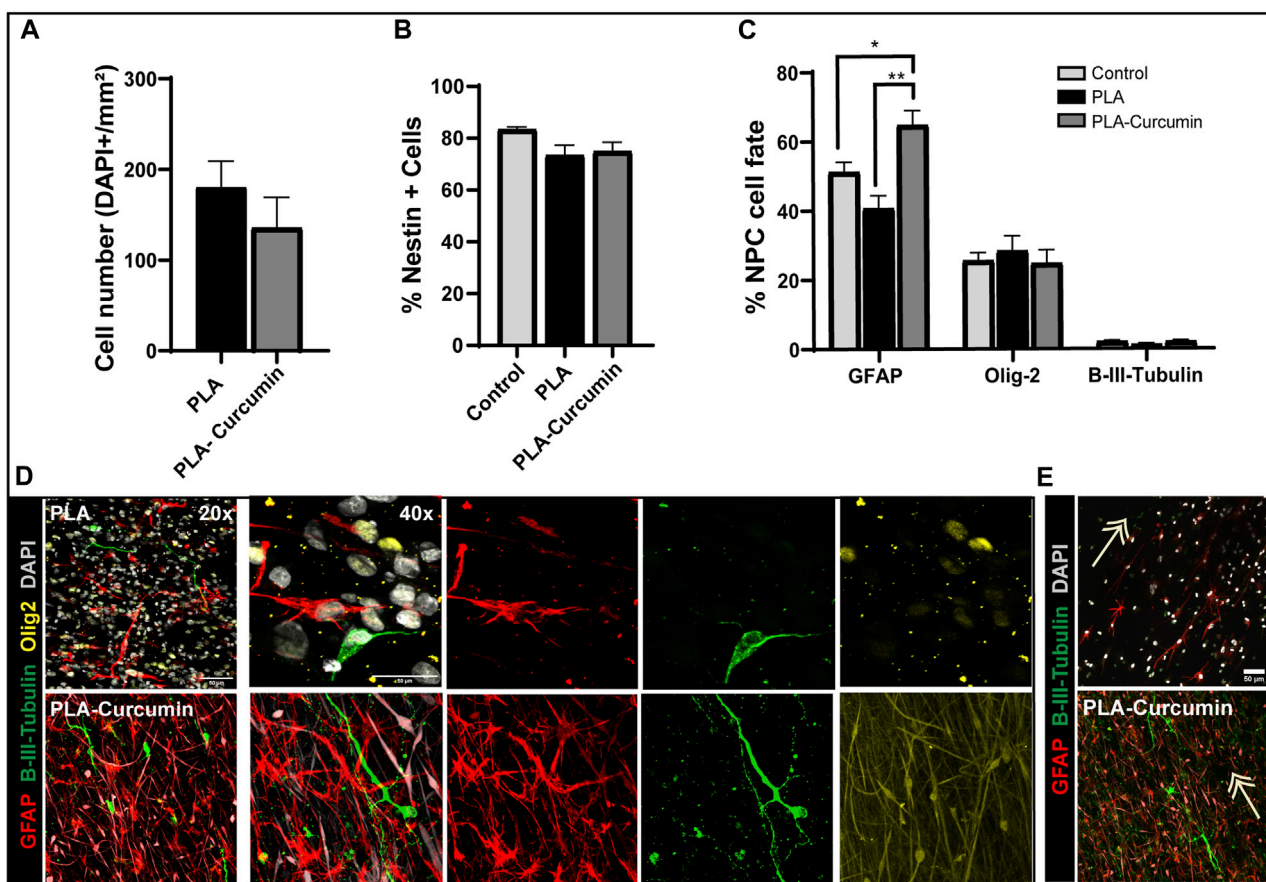


FIGURE 3

NPC adhesion and differentiation during growth on PLA and PLA-curcumin membranes. (A) Quantification of the absolute cell number, positive for DAPI staining, within the measured area (expressed in mm^2) of NPC seeded and attached to PLA or PLA-Curcumin membranes. (B) Quantification of the percentage of Nestin-positive NPC seeded on glass coverslip (control), PLA, or PLA-curcumin membranes for 3 days in growth medium. Data normalized by total cell number by quantifying DAPI nuclear staining. (C) Quantification of the percentage of astrocytes (positive for GFAP), oligodendrocytes (positive for Olig2), and neurons (positive for β -III tubulin) after 7 days of spontaneous differentiation of NPC in reduced growth factor media, seeded on PLA or PLA-curcumin membranes and control condition seeded on glass coverslips. Data normalized by total cell number by quantifying DAPI nuclear staining. $n = 3$ for each experiment. Data expressed as mean \pm SEM. * $p < 0.05$ and ** $p < 0.01$ determined by Ordinary one-way ANOVA, Sidak's multiple comparisons tests. (D) Representative images of immunofluorescence staining for β -III tubulin (green), GFAP (red), Olig-2 (yellow), and DAPI (grey) of quantifications shown in (C). Scale bars = 50 μm . (E) Representative images for the indicated co-labeling from PLA + NPC condition showing NPC orientation following the fibers distribution indicated with white arrows.

PLA and PLA-curcumin membranes enable NPC adhesion and migration

We next evaluated whether NPC can grow and attach on PLA membranes and if curcumin affects cell adhesion under growth conditions in the presence of growth factors compared to glass coverslips as a control substrate (Figure 3). First, the quantification of total cell number positive for DAPI nuclei staining attached to the PLA or PLA-Curcumin over a period of 3 days did not reveal any difference among conditions (Figure 3A). 73.37% \pm 3.82 of the NPC that attached and grew on the PLA membrane expressed Nestin, and we failed to see any significant difference in Nestin expression when compared to grown NPC on the PLA-curcumin membrane (74.86 \pm 3.57) or Control (82.40 \pm 2.87) (Figure 3B). This suggests that the majority of NPC exist in an undifferentiated state. To induce spontaneous differentiation, mitotic growth factors were removed from NPC cultured PLA and PLA-curcumin membranes over 7 days, using glass coverslips as a control substrate. Notably, NPC

cultured and attached to the PLA-Curcumin membrane exhibited a significant increase in astrocytic differentiation (GFAP-positive cells, red) compared to those on the PLA membrane and control (Figures 3C, D). However, we failed to observe significant differences in oligodendrocytic (Olig2-positive cells, yellow) or neuronal (β -III tubulin-positive cells, green) differentiation over the three substrates (Figures 3C, D). Upon closer examination of NPC distribution in the different conditions, it was observed that NPC grew over the PLA fibers following a parallel distribution as evidenced by the DAPI nuclear cell staining (Figure 3E, grey) highlighted with white arrows in any of the tested conditions. Both GFAP (red) and β -III tubulin-positive neurons also elongated following the fibers axis (Figure 3E, green, white arrows), with no significant differences induced by the presence of curcumin (data not shown).

Overall, the PLA membranes including or not Curcumin in cell growth conditions maintain the attached NPC in an undifferentiated stage, however, in the absence of mitotic factors the released curcumin promotes astroglia differentiation.

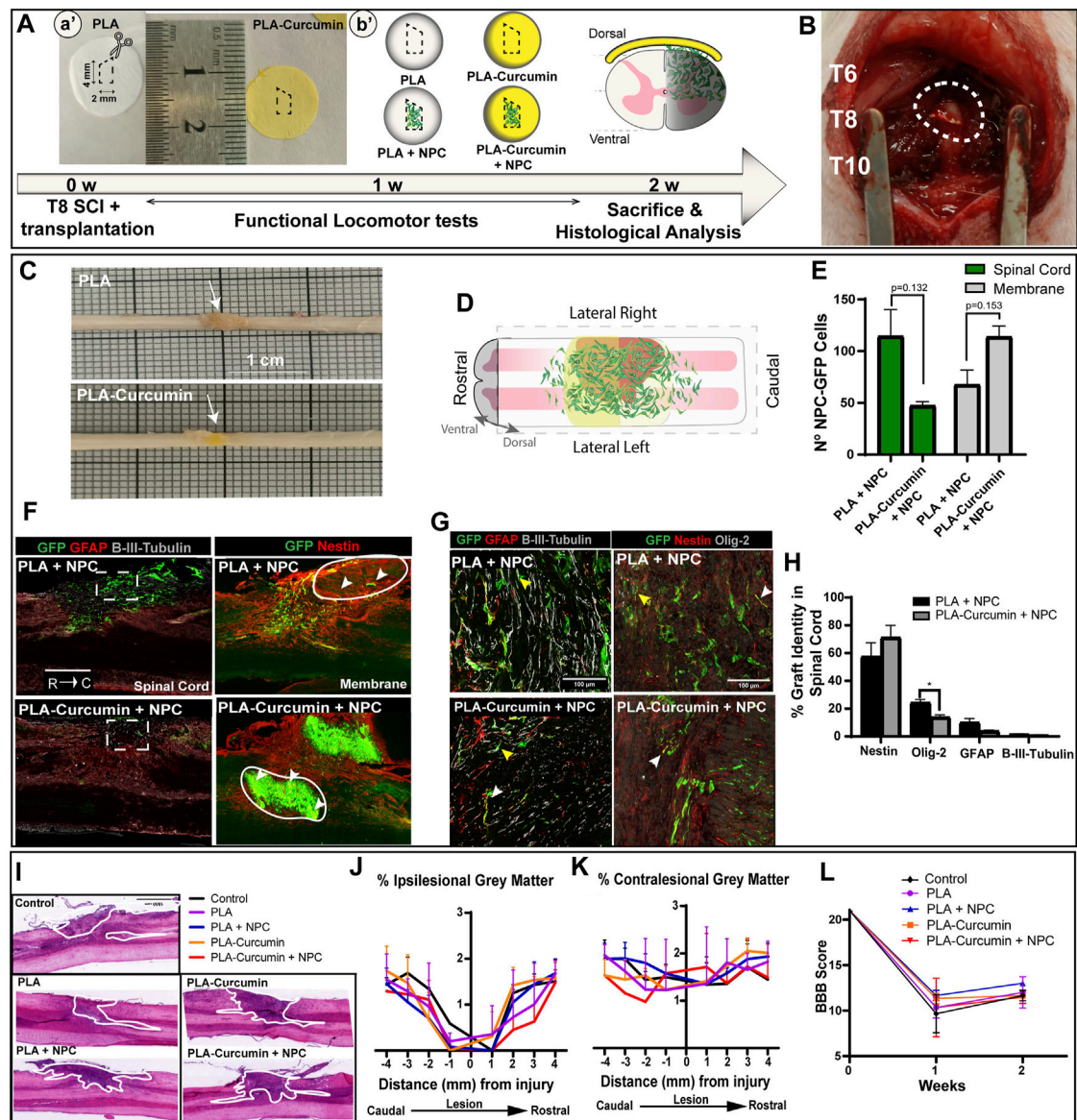


FIGURE 4

PLA and PLA-curcumin membranes as vehicles for NPC transplantation and treatment of SCI. **(A)** Scheme of the experimental workflow: **a'**: PLA (white disc) or PLA-curcumin (yellow disc) membranes pre-cut to a 2 × 4 mm size with an angle in the upper size as indicated with the dashed white line. **b'**: Membranes with or without GFP-overexpressing NPC attached were transplanted on the dorsal part of the spinal cord. **(B)** Representative image of membrane implantation over the T8 segment after lateral hemisection. **(C)** The harvested spinal cord samples demonstrated visible attachment of the membranes to the implanted area (indicated by arrows). **(D)** Graphical representation showing the longitudinal view of the spinal cord and the orientation used for the histological analysis performed. The expected migration of NPC from the implanted membrane into the injured area is also shown. **(E)** Quantification of the average number of grafted GFP-expressing NPC in the spinal cord tissue (green bar) or remaining on the membranes (grey bars). 61.73% of NPC transplanted on the PLA membrane (PLA+NPC) had invaded the spinal cord while only 31.34% of NPC transplanted are on the PLA-Curcumin membrane (PLA-Curcumin + NPC). Data expressed as mean ± SEM, *n* = 3 animals per group. **p* < 0.05, determined by unpaired *t*-test. **(F)** Longitudinal view of immunofluorescence staining for GFP-expressing NPC (green), GFAP or Nestin (red), and β-III tubulin (grey). GFP-expressing NPC invaded the spinal cord (left column) in PLA+NPC while in PLA-Curcumin + NPC group, they remained on the membrane (right column). The dashed white squares represent NPC-GFP at the injury site, circles indicate the position of the remaining membranes adhered to the spinal cord tissue and the white arrows indicate the location of GFP-expressing NPC. **(G)** Representative images of labeling for GFP-expressing NPC (green), GFAP or Nestin (red), β-III tubulin, or Olig-2 (grey). White and yellow arrows indicate the GFP-expressing NPC colocalization with GFAP, Nestin, and Olig-2 or β-III tubulin, respectively. **(H)** Quantification of the GFP-expressing NPC grafted into the spinal cord tissue that express Nestin (neural progenitor cell marker), Olig2 (oligodendrocyte marker), GFAP (astrocyte marker), or β-III tubulin (neuronal marker). **(I)** Representative images of H&E staining for one horizontal slice of one animal per group as indicated. The white line indicates the injury area in each condition. **(J)** Quantification of the preserved grey matter area at the ipsilesional side and the **(K)** contralesional side every mm segment for 4 mm caudally and 4 mm rostrally to the injury. **(L)** Functional locomotor BBB test analyses performed one and 2 weeks (1 w, 2 w in A) after injury.

Transplantation of NPC into the injured spinal cord using PLA and PLA-curcumin membranes

To test whether the generated electrospun membranes would support neuroprotection by sustained delivery of curcumin and NPC, electrospun membranes were transplanted into the injured area in an SCI model immediately after lateral hemisection. An injured non-treated control group was also included (Control). PLA (white) or PLA-curcumin (yellow) membranes were cut to a size of 2×4 mm to match the laminectomy area (as represented in Figures 4A, 4a'). Matrigel-coated PLA and PLA-curcumin membranes with and without attached NPC overexpressing green fluorescent protein (NPC-GFP) (green; Figures 4A, 4b', left image) were then implanted to cover the injured area (Figure 4B). Animals were sacrificed, perfused and spinal cord dissected for histological analysis 2 weeks after implantation. The implanted membranes were found attached and well preserved at the implanted area (Figure 4C, white arrow). A 2-week interval following the injury was used as an early time point to enable a comprehensive evaluation of critical factors to determine the potential suitability of the membranes for further long-term applications, including i) the ability of the membrane to attach and integrate effectively into the affected area without contributing to further tissue damage; ii) the degree of graft survival and migration exhibited by NPC from the biomaterial into the spinal cord; iii) and its neuroprotective capabilities.

We first evaluated whether PLA and PLA-Curcumin membranes enable cell migration and engraftment upon transplantation in an acute state. We monitored the GFP expression by NPC 2 weeks after SCI from the ventral to the dorsal side, as graphically represented in Figure 4D. We quantified the existence of GFP-overexpressing NPC using ImageJ into the spinal cord or in the membrane (using the last dorsal slices) and represented it as an average number per slice per animal (Figure 4E). When transplanting NPC on the PLA membrane (PLA+NPC), $61.76\% \pm 23.76\%$ invaded the spinal cord with 38.23 ± 15.31 remaining on the membrane. However, on the PLA-Curcumin membrane (PLA-Curcumin + NPC), we found a lower percentage of cells invading the spinal cord ($31.34\% \pm 3.40\%$, with $68.66\% \pm 9.70\%$ remaining on the membrane). Representative images of NPC-GFP survival after acute transplantation at the injury site in the spinal cord tissue (Figure 4F, left column dashed square) and on the membrane (Figure 4F, right column, white circle represent the membrane while the white arrows indicate NPC-GFP). Of note, these differences failed to reach statistical significance. While the GFP-overexpressing NPC transplanted on the membranes mainly located to the injury site (location of the implanted membrane indicated within the white circled area), we observed NPC spread up to 3 mm caudally and rostrally to the injury. Both groups displayed the distribution of NPC from the dorsal to the ventral side, reaching a maximum depth of $1280 \pm 130.4 \mu\text{m}$ from the dorsal side. Overall, only 2 weeks after implantation, PLA membranes enable NPC migration of about 61.76% of the surviving NPC. However, PLA-curcumin may act to inhibit NPC migration from the membrane and delay NPC engraftment within the SCI. Therefore, the selection of a candidate drug to be incorporated in these membranes should

be carefully evaluated, as it may have a direct impact on the migration of transplanted cells.

When assessing the graft 2 weeks after implantation, non-significant alterations were observed in the stem cell (Nestin-positive cells), neural (β -III tubulin), and astrocytic (GFAP-positive cells) fate of NPC when comparing the use of PLA and PLA-curcumin membrane (Figures 4G, H; white and yellow arrows indicate the GFP-expressing NPC colocalization with GFAP, Nestin, and Olig-2 or β -III tubulin, respectively). However, NPC transplanted on the PLA-curcumin membrane (13.97 ± 1.63) displayed a significant reduction in the number of Olig-2 positive cells when compared to the PLA membrane (20.92 ± 2.24), suggesting the inhibition of oligodendrocytic differentiation of NPC.

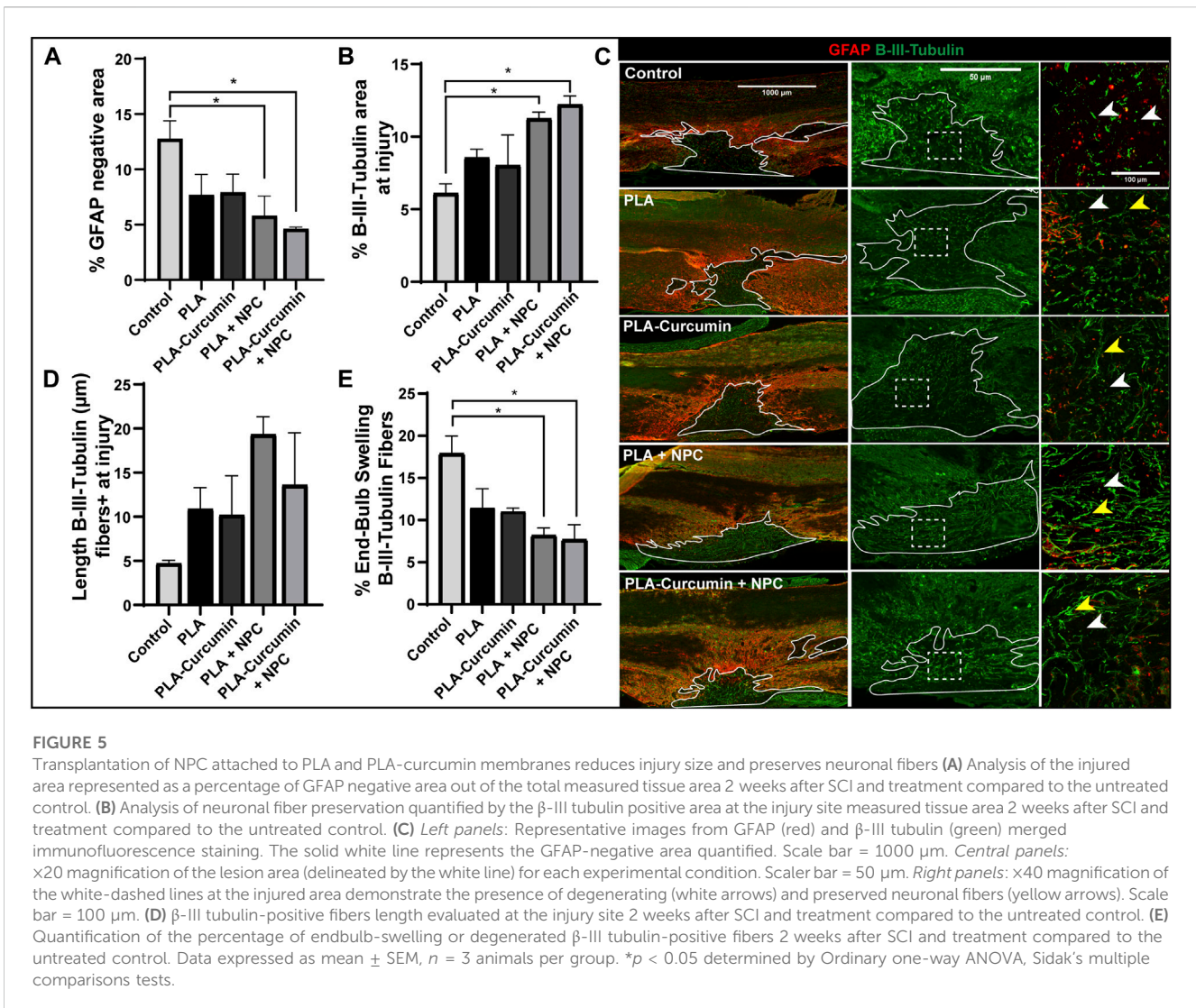
Subsequently, hematoxylin and eosin (H&E) staining of the spinal cords' horizontal sections, including the epicenter of the injured area, provided a general overview of the tissue damage distribution (Figure 4I, representative images). Quantification of the preserved grey matter in the H&E-stained sliced tissue at the ipsilesional (Figure 4J, left panel) and contralesional areas (Figure 4K, right panel) failed to reveal any differences between the five treatment groups. Basso, Beattie, and Bresnahan (BBB) open-field locomotor scale test one and 2 weeks after surgery reveals no significant differences between the various treatments (Figure 4L), indicating that membrane implantation does not have any early detrimental impact on the locomotor function of the rats. These results suggest that using PLA membranes as a carrier of small drugs, such as curcumin, or NPC transplantation did not elicit any additional adverse effects.

Overall, this histological analysis suggests that the electrospun PLA membranes do not induce any additional damage to the injured spinal cord and provide a controlled delivery system for minimally invasive NPC transplantation.

Transplantation of NPC with PLA or PLA-curcumin membranes reduces the injured area and increases neuronal fiber preservation

We lastly performed the additional immunohistochemical analysis at the injury epicenter to evaluate the effects of the transplanted NPC and/or curcumin release by the PLA membranes on control of the injury size/expansion and the preservation of the neuronal fibers compared to the untreated control group. The analysis of the injury size, measured as the GFAP negative area in horizontal tissue sections, revealed that transplantation of NPC on PLA or PLA-curcumin membranes significantly prevented the enlargement of the injured area through a comparison with the untreated control group (Figure 5A and representative images in Figure 5C, red). PLA and PLA-curcumin membrane implantation without attached NPC prompted a similar level of injured area inhibition; however, these values did not reach statistical significance (Figure 5A).

By staining neuronal fibers at the injury epicenter on the dorsal side with β -III tubulin, we evaluated neuronal tract preservation through the GFAP-negative tissue area. Transplantation of NPC



with the PLA and PLA-curcumin membranes induced significantly higher β -III tubulin-positive staining compared to the untreated control group (Figure 5B and representative images in Figure 5C, yellow arrows highlight preserved fibers in green), suggesting greater neuronal tract preservation. Meanwhile, PLA and PLA-curcumin membrane implantation without attached NPC failed to induce statistically significant increases in neuronal tract preservation (Figure 5B). PLA membranes with or without curcumin/NPC supported an upward trend in axonal lengths compared to the untreated control group (Figure 5D); however, these changes failed to reach statistical significance.

Of note, transplantation of NPC attached to PLA and PLA-curcumin membranes prompted significantly fewer degenerating fibers than the untreated control group (Figure 5E), which we evaluated by quantifying degenerating fibers displaying an endbulb-swelling morphology (with an end roundness factor greater than 0.7) (Figure 5C, indicated with white arrows). PLA and PLA-curcumin membranes alone may also have a role in preserving premature degeneration of neural fibers compared to the control group; however, the decreases in degeneration failed to reach significance.

Overall, we observed a neuroprotective effect when transplanting NPC attached to electrospun PLA membranes independent of the presence of curcumin in the tested conditions.

Discussion

In this study, we report the generation of electrospun PLA membranes that provide a versatile platform for supporting NPC transplantation and sustained drug delivery such as curcumin, for combinatorial treatment approaches in SCI.

We selected electrospinning as a simple but versatile technique to generate nanofibers; overall, the process employs low-cost equipment and has broad applicability and huge industrialization prospects with high batch-to-batch reproducibility [as reviewed by (Ding et al., 2019)]. Electrospinning supports the generation of nanofibers from different biomaterials to produce a diverse range of fiber diameters (ranging from several to several hundred nanometers) that mimic the axonal diameter of the mammalian spinal cord. Control over the range of sizes can

also support the development of fibers that resemble fibrous proteins to mimic extracellular matrix structures, which provides final flexibility and hardness compatible with soft tissue such as the spinal cord (Shu et al., 2019). Here, we employed electrospun PLA membranes with a thickness of a hundred micrometers, which ensured high flexibility and sufficient lightness to avoid tissue deformity upon surface deposition over spinal cord tissue. The electrospun PLA membranes can be easily manipulated, can adapt to the shape of the implanted area, and demonstrate high tolerability in direct contact with the spinal cord, even in the case of lost dura mater integrity (showing no additional tissue degeneration compared to non-transplanted animals) (Shu et al., 2019).

The generated membrane nanofibers provide structural support for endogenous tissue remodeling and functional neuronal regeneration close to the implanted area (Shu et al., 2019). In addition, the PLA nanofibers serve as an ectopic cell carrier supporting cell adhesion, growth, guidance, and neuronal differentiation, as we (and others) have previously demonstrated for NPC (Li et al., 2021; Cuenca-Ortola et al., 2022; Li et al., 2022).

Electrospun PLA membranes can also serve as a versatile drug delivery system for neuronal repair applications (Li et al., 2022). In addition, the PLA substrates generated through electrospinning were selected due to their non-toxicity properties, good biocompatibility with spinal cord tissue, and suitability for NPC transplantation and small drug delivery (Lasprilla et al., 2012; Li et al., 2021; Li et al., 2022; Feng et al., 2023). However, other polymers such as PLGA and PCL could also be suitable as carriers to deliver curcumin *via* electrospinning. PCL, for instance, could provide quicker polymer degradation, while PLGA could offer a tunable degradation rate (Scaffaro et al., 2017; Dias et al., 2022).

The use of electrospinning substrates allows for the introduction of a geometric pattern due to the aligned nanofibers, which can guide and orient the cells seeded on its surface, as well as the neurites, by mechanically constricting the cells (Lee et al., 2011; Zhu et al., 2015). This topographic interaction between cells and the biomaterial is mainly based on adhesion and mechanical transduction signals (Tsimbouri et al., 2014; Amani et al., 2019). Aligned nanofibers are capable of guide the axonal growth more efficiently than in flat substrate or on randomly oriented nanofibers (Lee et al., 2011; Wang et al., 2011; Zhu et al., 2015). We found that aligned electrospun fibers on the PLA membranes provide contact guidance to the seeded NPC, independently of the presence of Curcumin, resulting in both, alignment and elongation of either, neural and glial cells, positive for beta-III tubulin or GFAP respectively.

We functionalized electrospun PLA membranes during electrospinning by including curcumin solubilized in DMSO in the electrospinning solution. This process modifies the surface topography of the nanofibers, as previously described in comparable manufacturing procedures (Snetkov et al., 2022), which can allow control over surface roughness to enhance the adsorption of extracellular matrix proteins and thus improve cell adherence (Ibrahim and Klingner, 2020). As the PLA-curcumin membranes supported a reduced NPC migration into the injured spinal cord, we hypothesized that this surface modification might increase NPC adhesion to the membrane. In addition, limited NPC migration could derive from the increased

expression of adhesion molecules in NPC induced by released curcumin (Karlstetter et al., 2011). PLA nanofibers fabricated to contain docosahexaenoic acid (DHX) and/or brain-derived neurotrophic factor (BDNF) (Liu et al., 2022) or Paclitaxel (Roman et al., 2016) display a similar surface topology to PLA-curcumin membrane nanofibers and possess a similar enhanced ability to guide and support axonal elongation in neuronal cultures and provide neuroprotection and enhanced neuroplasticity when implanted over hemisectioned spinal cords *in vivo* (Liu et al., 2022). Interestingly, the *in vitro* delivery of DHX or BDNF within electrospun PLA fibers follows a similar profile as the PLA-curcumin membrane fibers, with a linear, rapid delivery profile for the first week followed by a slower rate of delivery of the remaining cargo (Liu et al., 2022). We previously demonstrated that PLA nanofibers improved neurite growth and axonal guidance (Gisbert Roca et al., 2020; Gisbert Roca et al., 2021; Gisbert Roca et al., 2022), but as shown here, the addition of curcumin did not display any additive effect. Nevertheless, equivalent concentrations of sustained delivered curcumin from the PLA nanofibers could contribute to neuronal elongation and axonal growth in endogenous tissue; however, this phenomenon will need to be further evaluated in a longer-term study. One week after implantation, we failed to identify significant differences among the groups (including in the presence of curcumin) when evaluating neuronal fiber length. We also obtained comparable results in animals implanted with NPC-coated PLA/PLA-curcumin membranes independently of the number of NPC migrating into the spinal cord. Compared with PLA membranes without NPC, NPC-coated PLA/PLA-curcumin membranes displayed a significantly lower number of neuronal endbulb-swelling or degenerated retraction bulbs at the injured area, an increase in neuronal fiber preservation, and a lower injured area size, indicating an effect independent of the curcumin delivery. These results may suggest that the NPC provide paracrine trophic support, which does not require migration into the injury site since the presence of curcumin delayed their migration into the injured area; nevertheless, a potential additive neuroprotective effect of curcumin compensating for the limited number of engrafted cells as well as the long-term effect of the curcumin retained activity over NPC migration into the injury site requires further investigation.

Conclusion

We provide evidence that electrospun PLA membranes provide an advanced and flexible system for NPC implantation and local drug delivery, such as curcumin. Both, PLA and PLA-Curcumin electrospun membranes, maintain attached NPC in an undifferentiated stage when cultured in an enriched media. However, in the absence of mitotic factors, the released curcumin promotes astroglia differentiation. The implantation of PLA or PLA-Curcumin membranes covered by NPC over the spinal cord injured area significantly reduces the number of degenerating fibers and preserves the premature degeneration of host neural fibers without causing additional tissue damage.

Data availability statement

The original contributions presented in the study are included in the article/[Supplementary Material](#), further inquiries can be directed to the corresponding author.

Ethics statement

The animal study was approved by Animal Care and Use Committee of the Research Institute Prince Felipe (the approved procedure ID is: 2021/VSC/PEA/0032). The study was conducted in accordance with the local legislation and institutional requirements.

Author contributions

MS-M: Conceptualization, Data curation, Formal Analysis, Investigation, Methodology, Writing—original draft, Writing—review and editing. EG: Data curation, Supervision, Writing—review and editing. FG: Data curation, Formal Analysis, Methodology, Writing—original draft, Writing—review and editing. CM-R: Formal Analysis, Methodology, Writing—original draft, Writing—review and editing. MM: Supervision, Writing—original draft, Writing—review and editing. VM-M: Conceptualization, Data curation, Formal Analysis, Funding acquisition, Project administration, Supervision, Writing—original draft, Writing—review and editing.

Funding

The authors declare financial support was received for the research, authorship, and/or publication of this article. This research was funded by FEDER/Ministerio de Ciencia e Innovación—Agencia Estatal de Investigación (AEI) PID2021-1243590B-I100 (to VM-M) and PID2021-126612OB-I00 (to MM) funded by MCIN/AEI/10.13039/501100011033 and by ERDF A way of making Europe, as well as the RISEUP EU grant (Ref. 964562) from FetOpen H2020 program. FG and MM-P acknowledge financing from Vicerrectorado de Investigación de la Universitat

References

- Amani, H., Arzaghi, H., Bayandori, M., Dezfuli, A. S., Pazoki-Toroudi, H., Shafiee, A., et al. (2019). Controlling cell behavior through the design of biomaterial surfaces: a focus on surface modification techniques. *Adv. Mater. interfaces* 6 (13), 1900572. doi:10.1002/admi.201900572
- Anjum, A., Yazid, M. D. I., Fauzi Daud, M., Idris, J., Ng, A. M. H., Selvi Naicker, A., et al. (2020). Spinal cord injury: pathophysiology, multimolecular interactions, and underlying recovery mechanisms. *Int. J. Mol. Sci.* 21 (20), 7533. doi:10.3390/ijms21207533
- Barbosa, K. A., Rodrigues, I. C. P., Tamborlin, L., Luchessi, A. D., Lopes, É. S. N., and Gabriel, L. P. (2022). Rotary jet-spun curcumin-loaded poly L-lactic acid membranes for wound-healing applications. *J. Mater. Res. Technol.* 18, 3273–3282. doi:10.1016/j.jmrt.2022.03.136
- Bethea, J. R., Castro, M., Keane, R. W., Lee, T. T., Dietrich, W. D., and Yezierski, R. P. (1998). Traumatic spinal cord injury induces nuclear factor- κ B activation. *J. Neurosci.* 18 (9), 3251–3260. doi:10.1523/jneurosci.18-09-03251.1998
- Bierman-Duquette, R. D., Safarians, G., Huang, J., Rajput, B., Chen, J. Y., Wang, Z. Z., et al. (2022). Engineering tissues of the central nervous system: interfacing conductive

Politécnica de València (PAID-10-22). MS-M was supported by a grant from the AEI in the FPI program. Part of the equipment employed in this work was funded by Generalitat Valenciana and co-financed with ERDF funds (OP ERDF of Comunitat Valenciana 2014–2020) and the UE; Fondo Europeo de Desarrollo Regional (FEDER) incluido en el Programa Operativo FEDER de la Comunidad Valenciana 2014–2020.

Acknowledgments

The authors would like to thank Eric Lopez Mocholi for his technical support in the histological analysis and Stuart P. Atkinson for English editing.

Conflict of interest

The authors declare that the research was conducted in the absence of any commercial or financial relationships that could be construed as a potential conflict of interest.

The authors declared that they were an editorial board member of *Frontiers*, at the time of submission. This had no impact on the peer review process and the final decision.

Publisher's note

All claims expressed in this article are solely those of the authors and do not necessarily represent those of their affiliated organizations, or those of the publisher, the editors and the reviewers. Any product that may be evaluated in this article, or claim that may be made by its manufacturer, is not guaranteed or endorsed by the publisher.

Supplementary material

The Supplementary Material for this article can be found online at: <https://www.frontiersin.org/articles/10.3389/fbiom.2023.1298894/full#supplementary-material>

biomaterials with neural stem/progenitor cells. *Adv. Healthc. Mater* 11 (7), e2101577. doi:10.1002/adhm.202101577

Bogdanova, A., Pavlova, E., Polyanskaya, A., Volkova, M., Biryukova, E., Filkov, G., et al. (2023). Acceleration of electrospun PLA degradation by addition of gelatin. *Int. J. Mol. Sci.* 24 (4), 3535. doi:10.3390/ijms24043535

Bonilla, P., Hernandez, J., Giraldo, E., Gonzalez-Perez, M. A., Alastrue-Agudo, A., Elkhenany, H., et al. (2021). Human-induced neural and mesenchymal stem cell therapy combined with a curcumin nanoconjugate as a spinal cord injury treatment. *Int. J. Mol. Sci.* 22 (11), 5966. doi:10.3390/ijms22115966

Brown, A. R., and Martinez, M. (2019). Thoracic spinal cord hemisection surgery and open-field locomotor assessment in the rat. *J. Vis. Exp.* 2019, 148. doi:10.3791/59738

Chen, X., Zou, L. Q., Niu, J., Liu, W., Peng, S. F., and Liu, C. M. (2015). The stability, sustained release and cellular antioxidant activity of curcumin nanoliposomes. *Molecules* 20 (8), 14293–14311. doi:10.3390/molecules200814293

Collins, M. N., and Birkinshaw, C. (2013). Hyaluronic acid based scaffolds for tissue engineering—a review. *Carbohydr. Polym.* 92 (2), 1262–1279. doi:10.1016/j.carbpol.2012.10.028

- Cuenca-Ortola, I., Martínez-Rojas, B., Moreno-Manzano, V., García Castello, M., Monleon Pradas, M., Martínez-Ramos, C., et al. (2022). A strategy for magnetic and electric stimulation to enhance proliferation and differentiation of NPCs seeded over PLA electrospun membranes. *Biomedicines* 10 (11), 2736. doi:10.3390/biomedicines10112736
- Dias, J. R., Sousa, A., Augusto, A., Bártolo, P. J., and Granja, P. L. (2022). Electrospun polycaprolactone (PCL) degradation: an *in vitro* and *in vivo* study. *Polymers* 14 (16), 3397. doi:10.3390/polym14163397
- Ding, Y., Li, W., Zhang, F., Liu, Z., Zanjanzadeh Ezazi, N., Liu, D., et al. (2019). Electrospun fibrous architectures for drug delivery, tissue engineering and cancer therapy. *Adv. Funct. Mater.* 29 (2), 2852. doi:10.1002/adfm.201802852
- Dupraz, S., Hilton, B. J., Husch, A., Santos, T. E., Coles, C. H., Stern, S., et al. (2019). RhoA controls axon extension independent of specification in the developing brain. *Curr. Biol.* 29 (22), 3874–3886.e9. doi:10.1016/j.cub.2019.09.040
- Elkhenany, H., Bonilla, P., Giraldo, E., Alastrue Agudo, A., Edel, M. J., Vicent, M. J., et al. (2021). A hyaluronic acid demulose scaffold and polypyrrole-coated fibers carrying embedded human neural precursor cells and curcumin for surface capping of spinal cord injuries. *Biomedicines* 9 (12), 1928. doi:10.3390/biomedicines9121928
- Feng, C., Deng, L., Yong, Y. Y., Wu, J. M., Qin, D. L., Yu, L., et al. (2023). The application of biomaterials in spinal cord injury. *Int. J. Mol. Sci.* 24 (1), 816. doi:10.3390/ijms24010816
- Gisbert Roca, F., Andre, F. M., Mas Estelles, J., Monleon Pradas, M., Mir, L. M., and Martínez-Ramos, C. (2021). BDNF-gene transfected schwann cell-assisted axonal extension and sprouting on new PLA-PPy microfiber substrates. *Macromol. Biosci.* 21 (5), e2000391. doi:10.1002/mabi.202000391
- Gisbert Roca, F., Más Estellés, J., Monleón Pradas, M., and Martínez-Ramos, C. (2020). Axonal extension from dorsal root ganglia on fibrillar and highly aligned poly(lactic acid)-polypyrrole substrates obtained by two different techniques: electrospun nanofibers and extruded microfibers. *Int. J. Biol. Macromol.* 163, 1959–1969. doi:10.1016/j.ijbiomac.2020.09.181
- Gisbert Roca, F., Serrano Requena, S., Monleon Pradas, M., and Martínez-Ramos, C. (2022). Electrical stimulation increases axonal growth from dorsal root ganglia Co-cultured with schwann cells in highly aligned PLA-PPy-Au microfiber substrates. *Int. J. Mol. Sci.* 23 (12), 6362. doi:10.3390/ijms23126362
- Griffin, J. M., and Bradke, F. (2020). Therapeutic repair for spinal cord injury: combinatory approaches to address a multifaceted problem. *EMBO Mol. Med.* 12 (3), e11505. doi:10.15252/emmm.201911505
- Gu, X., Su, X., Jia, C., Lin, L., Liu, S., Zhang, P., et al. (2019). Sprouty1 regulates neurogenesis and survival of cortical neurons. *J. Cell. Physiol.* 234 (8), 12847–12864. doi:10.1002/jcp.27949
- Ibrahim, H. M., and Klingner, A. (2020). A review on electrospun polymeric nanofibers: production parameters and potential applications. *Polym. Test.* 90, 106647. doi:10.1016/j.polymtest.2020.106647
- Jeong, H. J., Yun, Y., Lee, S. J., Ha, Y., and Gwak, S. J. (2021). Biomaterials and strategies for repairing spinal cord lesions. *Neurochem. Int.* 144, 104973. doi:10.1016/j.neuint.2021.104973
- Joung, D., Truong, V., Neitzke, C. C., Guo, S. Z., Walsh, P. J., Monat, J. R., et al. (2018). 3D printed stem-cell derived neural progenitors generate spinal cord scaffolds. *Adv. Funct. Mater.* 28 (39), 1801850. doi:10.1002/adfm.201801850
- Karlstetter, M., Lippe, E., Walczak, Y., Moehle, C., Aslanidis, A., Mirza, M., et al. (2011). Curcumin is a potent modulator of microglial gene expression and migration. *J. Neuroinflammation* 8, 125. doi:10.1186/1742-2094-8-125
- Katoh, H., Yokota, K., and Fehlings, M. G. (2019). Regeneration of spinal cord connectivity through stem cell transplantation and biomaterial scaffolds. *Front. Cell. Neurosci.* 13, 248. doi:10.3389/fncel.2019.00248
- Khalil, M. M. H., Mahdy, H., Sabry, D. Y., and Ismail, E. H. (2014). Synthesis and characterization of some ternary metal complexes of curcumin with 1,10-phenanthroline and their anticancer applications. *J. Sci. Res.* 6 (3), 509–519. doi:10.3329/jsr.v6i3.18750
- Koffler, J., Zhu, W., Qu, X., Platoshyn, O., Dulin, J. N., Brock, J., et al. (2019). Biomimetic 3D-printed scaffolds for spinal cord injury repair. *Nat. Med.* 25 (2), 263–269. doi:10.1038/s41591-018-0296-z
- Kuramoto, Y., Takagi, T., Takeda, Y., Rajbhandari, S., Yoshida, Y., Nakagomi, T., et al. (2022). Identification of novel multipotent stem cells in mouse spinal cord following traumatic injury. *Stem Cells Dev.* 31 (17–18), 555–568. doi:10.1089/scd.2021.0297
- Lampe, K. J., Bjugstad, K. B., and Mahoney, M. J. (2010). Impact of degradable macromer content in a poly (ethylene glycol) hydrogel on neural cell metabolic activity, redox state, proliferation, and differentiation. *Tissue Eng. Part A* 16 (6), 1857–1866. doi:10.1089/ten.tea.2009.0509
- Lasprilla, A. J., Martínez, G. A., Lunelli, B. H., Jardini, A. L., and Filho, R. M. (2012). Poly-lactic acid synthesis for application in biomedical devices - a review. *Biotechnol. Adv.* 30 (1), 321–328. doi:10.1016/j.biotechadv.2011.06.019
- Lee, Y. S., Collins, G., and Arinzech, T. L. (2011). Neurite extension of primary neurons on electrospun piezoelectric scaffolds. *Acta biomater.* 7 (11), 3877–3886. doi:10.1016/j.actbio.2011.07.013
- Li, Y., Dong, T., Li, Z., Ni, S., Zhou, F., Alimi, O. A., et al. (2022). Review of advances in electrospinning-based strategies for spinal cord regeneration. *Mater. Today Chem.* 24, 100944. doi:10.1016/j.mtchem.2022.100944
- Li, Z., Wang, Q., Hu, H., Zheng, W., and Gao, C. (2021). Research advances of biomaterials-based microenvironment-regulation therapies for repair and regeneration of spinal cord injury. *Biomed. Mater.* 16, 052002. doi:10.1088/1748-605X/ac1d3c
- Liu, Z. H., Huang, Y. C., Kuo, C. Y., Chuang, C. C., Chen, C. C., Chen, N. Y., et al. (2022). Co-delivery of docosahexaenoic acid and brain-derived neurotrophic factor from electrospun aligned core-shell fibrous membranes in treatment of spinal cord injury. *Pharmaceutics* 14 (2), 321. doi:10.3390/pharmaceutics14020321
- Meijering, E., Jacob, M., Sarria, J. C., Steiner, P., Hirling, H., and Unser, M. (2004). Design and validation of a tool for neurite tracing and analysis in fluorescence microscopy images. *Cytom. A* 58 (2), 167–176. doi:10.1002/cyto.a.20022
- More, S. V., Koppula, S., Kim, I. S., Kumar, H., Kim, B. W., and Choi, D. K. (2012). The role of bioactive compounds on the promotion of neurite outgrowth. *Molecules* 17 (6), 6728–6753. doi:10.3390/molecules17066728
- Narouiepour, A., Ebrahimzadeh-Bideskan, A., Rajabzadeh, G., Gorji, A., and Negah, S. S. (2022). Neural stem cell therapy in conjunction with curcumin loaded in niosomal nanoparticles enhanced recovery from traumatic brain injury. *Sci. Rep.* 12 (1), 3572. doi:10.1038/s41598-022-07367-1
- Patel, S. S., Acharya, A., Ray, R. S., Agrawal, R., Raghuvanshi, R., and Jain, P. (2019). Cellular and molecular mechanisms of curcumin in prevention and treatment of disease. *Crit. Rev. Food Sci. Nutr.* 60 (6), 887–939. doi:10.1080/10408398.2018.1552244
- Pinelli, F. F., Veneruso, V., Petillo, E., Raghunath, M., Perale, G., Veglianesi, P., et al. (2022). Biomaterial-mediated factor delivery for spinal cord injury treatment. *Biomedicines* 10, 1673. doi:10.3390/biomedicines10071673
- Ranjeth Kumar Reddy, T., and Kim, H. J. (2018). Mechanical, optical, thermal, and barrier properties of poly (lactic acid)/curcumin composite films prepared using twin-screw extruder. *Food Biophys.* 14 (1), 22–29. doi:10.1007/s11483-018-9553-4
- Raynald, R., Shu, B., Liu, X. B., Zhou, J. F., Huang, H., Wang, J. Y., et al. (2019). Polypyrrole/poly(lactic acid) nanofibrous scaffold cotransplanted with bone marrow stromal cells promotes the functional recovery of spinal cord injury in rats. *CNS Neurosci. Ther.* 25 (9), 951–964. doi:10.1111/cns.13135
- Requejo-Aguilar, R., Alastrue-Agudo, A., Cases-Villar, M., Lopez-Mocholi, E., England, R., Vicent, M. J., et al. (2017). Combined polymer-curcumin conjugate and ependymal progenitor/stem cell treatment enhances spinal cord injury functional recovery. *Biomaterials* 113, 18–30. doi:10.1016/j.biomaterials.2016.10.032
- Ribeiro, C., Sencadas, V., Costa, C. M., Gómez Ribelles, J. L., and Lanceros-Méndez, S. (2011). Tailoring the morphology and crystallinity of poly(L-lactide acid) electrospun membranes. *Sci. Technol. Adv. Mater.* 12 (1), 015001. doi:10.1088/1468-6996/12/1/015001
- Roman, J. A., Reucroft, I., Martin, R. A., Hurtado, A., and Mao, H. Q. (2016). Local release of Paclitaxel from aligned, electrospun microfibers promotes axonal extension. *Adv. Healthc. Mater.* 5 (20), 2628–2635. doi:10.1002/adhm.201600415
- Santhosh, K. T., Alizadeh, A., and Karimi-Abdolrezaee, S. (2017). Design and optimization of PLGA microparticles for controlled and local delivery of Neuregulin-1 in traumatic spinal cord injury. *J. Control. Release* 261, 147–162. doi:10.1016/j.jconrel.2017.06.030
- Scaffaro, R., Lopresti, F., Sutura, A., Botta, L., Fontana, R. M., and Gallo, G. (2017). Plasma modified PLA electrospun membranes for actinorhodin production intensification in *Streptomyces coelicolor* immobilized-cell cultivations. *Colloids Surfaces B Biointerfaces* 157, 233–241. doi:10.1016/j.colsurfb.2017.05.060
- Schnell, E., Klinkhammer, K., Balzer, S., Brook, G., Klee, D., Dalton, P., et al. (2007). Guidance of glial cell migration and axonal growth on electrospun nanofibers of poly-ε-caprolactone and a collagen/poly-ε-caprolactone blend. *Biomaterials* 28 (19), 3012–3025. doi:10.1016/j.biomaterials.2007.03.009
- Shin, J. H., and Kang, H. W. (2018). The development of gelatin-based bio-ink for use in 3D hybrid bioprinting. *Int. J. Precis. Eng. Manuf.* 19, 767–771. doi:10.1007/s12541-018-0092-1
- Shu, B., Sun, X., Liu, R., Jiang, F., Yu, H., Xu, N., et al. (2019). Restoring electrical connection using a conductive biomaterial provides a new therapeutic strategy for rats with spinal cord injury. *Neurosci. Lett.* 692, 33–40. doi:10.1016/j.neulet.2018.10.031
- Snetkov, P., Morozkina, S., Olekhovich, R., and Uspenskaya, M. (2022). Electrospun curcumin-loaded polymer nanofibers: solution recipes, process parameters, properties, and biological activities. *Mater. Adv.* 3 (11), 4402–4420. doi:10.1039/d2ma00440b
- Sun, Y., Yang, C., Zhu, X., Wang, J. J., Liu, X. Y., Yang, X. P., et al. (2019). 3D printing collagen/chitosan scaffold ameliorated axon regeneration and neurological recovery after spinal cord injury. *J. Biomed. Mater. Res. Part A* 107 (9), 1898–1908. doi:10.1002/jbm.a.36675
- Torres-Espin, A., Santos, D., Gonzalez-Perez, F., del Valle, J., and Navarro, X. (2014). Neurite-J: an image-J plug-in for axonal growth analysis in organotypic cultures. *J. Neurosci. Methods* 236, 26–39. doi:10.1016/j.jneumeth.2014.08.005
- Tsimbouri, P. M., McNamara, L. E., Alakpa, E. V., Dalby, M. J., and Turner, L. A. (2014). “Cell–material interactions,” in *Tissue engineering* (Elsevier), 217–251.

- Tsintou, M., Dalamagkas, K., and Seifalian, A. M. (2015). Advances in regenerative therapies for spinal cord injury: a biomaterials approach. *Neural Regen. Res.* 10 (5), 726–742. doi:10.4103/1673-5374.156966
- Wang, Y., Zhao, Z., Zhao, B., Qi, H. X., Peng, J., Zhang, L., et al. (2011). Biocompatibility evaluation of electrospun aligned poly (propylene carbonate) nanofibrous scaffolds with peripheral nerve tissues and cells *in vitro*. *Chin. Med. J.* 124 (15), 2361–2366.
- Zhang, M., Li, X., Li, S., Liu, Y., and Hao, L. (2016). Electrospun poly(l-lactide)/zein nanofiber mats loaded with *Rana chensinensis* skin peptides for wound dressing. *J. Mater. Sci. Mater. Med.* 27 (9), 136. doi:10.1007/s10856-016-5749-7
- Zhao, T., Jing, Y., Zhou, X., Wang, J., Huang, X., Gao, L., et al. (2018). PHBV/PLA/Col-based nanofibrous scaffolds promote recovery of locomotor function by decreasing reactive astrogliosis in a hemisection spinal cord injury rat model. *J. Biomed. Nanotechnol.* 14 (11), 1921–1933. doi:10.1166/jbn.2018.2622
- Zholudeva, L. V., and Lane, M. A. (2019). Transplanting cells for spinal cord repair: who, what, when, where and why? *Cell. Transplant.* 28 (4), 388–399. doi:10.1177/0963689718824097
- Zhu, W., Masood, F., O'Brien, J., and Zhang, L. G. (2015). Highly aligned nanocomposite scaffolds by electrospinning and electrospraying for neural tissue regeneration. *Nanomedicine Nanotechnol. Biol. Med.* 11 (3), 693–704. doi:10.1016/j.nano.2014.12.001
- Zipser, C. M., Cragg, J. J., Guest, J. D., Fehlings, M. G., Jutzeler, C. R., Anderson, A. J., et al. (2022). Cell-based and stem-cell-based treatments for spinal cord injury: evidence from clinical trials. *Lancet Neurol.* 21 (7), 659–670. doi:10.1016/S1474-4422(21)00464-6
- Zou, Y., Ma, D., Shen, H., Zhao, Y., Xu, B., Fan, Y., et al. (2020). Aligned collagen scaffold combination with human spinal cord-derived neural stem cells to improve spinal cord injury repair. *Biomaterials Sci.* 8 (18), 5145–5156. doi:10.1039/d0bm00431f